Metal-Addenda Substitution in Plenary Polyoxometalates and in Their Modular Transition Metal Analogues

Charlotte Simms,[a] Aleksandar Kondinski,*[a] and Tatjana N. Parac-Vogt[a]

Abstract: For decades, the formal metal addenda substitution in the matrix of bulk metal oxides has been a prolific strategy to develop numerous (non-)stochiometric all-inorganic compounds with tunable electronic and magnetic properties and broad technological applications. In contrast to bulk mixed-metal oxides, the formal metal-addenda substitution in their molecular equivalents typically leads to stoichiometrically precise mixed-metal cluster formulations which retain the overall structural topology of the monometallic archetype, but exhibit pronounced differences in terms of reactivity and spectroscopic properties. These mixed-metal molecular metal oxides often show complex configurational isomerism that has been the subject of many experimental and theoretical studies. The mixed-addenda metal-oxo clusters are most prominent among the classical plenary (i.e. "saturated") polyoxometalate (POMs) archetypes, which have emerging applications in homogeneous catalysis and material science (e.g. formation of open frameworks) and have also been explored in heterogeneous metal organic framework (MOF) catalysts. Therefore, this article provides comprehensive theoretical and experimental insights into the isomer problem of mixed-addenda molecular metal oxides and their applications.

1. Introduction

Metal oxides are the most common materials in the Earth's crust, and as such, human's exploration and gradual understanding of their properties has eventually prompted many technological and cultural advances over human history.[1–3] Over the past centuries much effort has been invested into understanding the atomistic and electronic properties of the metal oxides, whilst at the same time, many different synthetic protocols have been developed that allow convenient material preparation with structural, stoichiometric, and morphologic control at the nanoscale. Substitution of metal centers within the matrix of these bulk one, two- and three-dimensional materials has been a common strategy for the formation of mixed metal oxides (e.g. ternary or quaternary) that, depending on the degree of metal substitution, can exhibit tailored properties suitable to address custom applications. Such materials are typically developed via conventional wet or solid-state chemical synthesis[4] or atomic layer deposition techniques,[5] and effectively expand the applications of metal oxides in many emerging areas such as heterogeneous catalysis,[6,7] functional materials,[8] nanoelectronics,[9] energy-storing materials,[10] and others.

[a] Miss Charlotte Simms, Dr. Aleksandar Kondinski, Prof. Dr. Tatjana N. Parac-Vogt
Department of Chemistry, KU Leuven
Celestijnenlaan 200F 3001 Leuven, Belgium
E-mail: aleksandar.kondinski@kuleuven.be
Webpage: http://www.kondinski.com/
Phone: +32 16 37 29 41

In parallel to the development of bulk metal oxide chemistry, the past century has also seen remarkable developments in the chemistry of molecular metal oxides.[11–13] Molecular metal oxides are typically referred to as "zero-dimensional" metal oxides and span the scale of a few nanometers (most commonly around 1 nm). As discrete species, the molecular metal oxides have cluster-like features, adopt atomistically precise topologies and can be synthesised in a well-controlled manner. Polyoxometalates (POMs) are one of the most complex, representative and developed classes of molecular metal oxides exhibiting rich structural versatility.[14–16] Classical POMs typically consist of early transition metals in high oxidation states (mainly V, Nb, Ta, Mo, and W).[17] Additionally, over the past decades there has been significant reports of POMs built of late transition metals (Cu, Ni, Pd, Pt, and Au),[18] and actinide based POMs (e.g. U and Np).[19] Depending on their composition, POMs can adopt all-inorganic or hybrid (bio)organic-inorganic archetypes. Monometallic POMs that are based solely on metal addenda element (also rarely referred to as "peripheral") and oxo ligands are commonly referred to as isoPOMs and prominent examples are the Lindqvist structure and the decavanadates. On the other hand, POMs that contain (typically p-block) hetero-groups are referred to as heteroPOMs, with the Keggin the most well-known example (see Figure 1.a). Hybrid POMs can be further functionalized with various organic moieties, some of which have the possibility to undergo further (post-)functionalization.[20] Functionalization with organic materials and the broad scope of elements that can form POMs, eventually loosens the formal classification between these materials since many other transition metal analogues can build similar polynuclear metal-oxo clusters.[13] The hexazirconate cores[21] are a prominent example

Charlotte Simms studied Biochemistry and Biological Chemistry at the University of Nottingham, UK and then an MSc Chemistry at KU Leuven, Belgium. She completed an internship in the lab of Bioinorganic Chemistry at KU Leuven, focusing on Zr-metal organic frameworks, and her MSc thesis, focusing on the reactivity of bimetallic MOFs. As an FWO PhD Fellow, she is now working under the supervision of Prof. Parac-Vogt studying variations in bimetallic MOFs for use as artificial proteases.

Aleksandar Kondinski studied chemistry at Jacobs University Bremen. During his graduate studies at the same university he familiarized himself with polyoxometalate synthesis and characterization. Under the mentorship of Professor Thomas Heine he contributed to the theoretical description of polyoxometalates and graduated in 2016. After a postdoc stage at RWTH Aachen with Prof. Paul Kögerler and Dr. Monakhov he continued as an FWO postdoctoral fellow in the group of Prof. Parac-Vogt. His research interests lay in the domain of advanced polyoxometalates for nanoelectronics (i.e. "POMtronics") and for catalytical applications.

Tatjana Parac-Vogt is a full professor of chemistry at KU Leuven, Belgium. She studied chemistry at the University of Belgrade, former Yugoslavia, and obtained her PhD from Iowa State University in Ames, USA. Following her PhD, she performed post-doctoral research at the University of California at Berkeley in the group of Professor Ken Raymond. After that she spent two years in Germany as an Alexander von Humboldt Fellow, before moving to KU Leuven in 2000, where she is currently the head of the Laboratory of Bioinorganic Chemistry. She actively promotes gender and cultural diversity in the working environment.

of the later and are well-known for their role as functional nodes in the construction of metal-organic frameworks (MOFs).[22]

In this minireview we discuss the concept of mixed-addenda plenary (i.e. saturated or defect-free) POMs and MOF-constructing analogues, from the perspective of configurational isomerism as stipulated by the implementations of Pólya's theory.[23,24] In this regard, we review the substitution in well-known hexametalate, decametalate and dodecametalate archetypes where the metal centres describe the corners of virtual octahedron $\{M_{6-x}M'_x\}$, edge-sharing octahedra $\{M_{10-x}M'_x\}$ and a (quasi-)cuboctahedron $\{M_{12-x}M'_x\}$ respectively (Figure 1.a). The spatial arrangement of metal centres and their substitution leads to essentially the same or similar isomer enumeration and isomer configuration principles. Many possible bimetallic variations can be derived, based on the type and combination of metal materials incorporated, leading to specific physicochemical properties, stability orders, and applications. Following this, we review how the choice of synthetic strategy influences the construction of the mixed-addenda archetypes, ratio, and isomer abundance within the well-defined isomer sets, as well as how the properties of the mixed-addenda clusters differ from those of the monometallic species that retain the same archetype. We substantiate the discussion with significant contributions from density functional theory (DFT) studies in order to provide a broader and holistic understanding of the subject that has the potential to aid rational and computer-aided synthesis design of stable mixed-addenda metal-oxo clusters with desired (photo)redox properties, asymmetric Lewis acid-base catalytic sites, and spatial modularity.

2. Mixed addenda hexametalates

Interconnection of metal centres into discrete octahedral species depends on the connectivity of the available bridging oxo ligands. When μ_2-O bridging ligands are used, octahedral $\{M_6O_{12}\}$ topologies are constructed. On the other hand, when μ_3-O bridging ligands are used they result in octahedral $\{M_6O_8\}$ topology. Group V and Group VI metals typically build $\{M_6O_{12}\}$ octahedra that encapsulate the oxo ligand (i.e. μ_6-O), while each addenda centre is terminated by a single η-O ligand, leading to the well-known $\{M_6O_{19}\}$ Lindqvist structure (see Figure 1.b). On the other hand, the $\{M_6O_8\}$ topology is more compatible among group IV oxometalates, where some particular elements (e.g. Zr and Hf) can adopt larger coordination spheres. To achieve a full coordination sphere around the addenda centres, twelve carboxylate R-COO$^-$ ligand bridge in μ_2-fahsion leading to the $\{M_6O_8L_8\}$ topology (Figure 1.c). As the addenda centres in both cases are arranged in octahedral fashion, both systems share the same configurational space upon formal metal addenda substitution (Figure 1.d).

2.1 Lindqvist-type $\{M_{6-x}M'_xO_{19}\}$ systems

The small cluster $\{M_6O_{19}\}$, known as Lindqvist iso-POM, is most commonly formed of Mo, W, Nb, or Ta octahedra and is well-suited for formal metal substitutions.[17,19,25–28] Thus, tuning of specific electronic and photocatalytic responses can be achieved. The hypothetical fully-inorganic $[V_6O_{19}]^{8-}$ cluster would count as significantly better visible light driven photocatalyst in contrast to its heavier Nb and Ta analogues,[29–31] however, until date fully-inorganic and solution stable Lindqvist $[V_6O_{19}]^{8-}$ have not been isolated nor confirmed to be plausible synthetic targets based on theoretical calculations considering the Hoffmann-Schleyer-Schaefer criteria.[32] This instability stems from a high charge density of ρ_{CD} = 31.738 C·mol·dm^3, compared to 8.403 C·mol·dm^3 for the more stable $\{Mo_6O_{19}\}$ cluster, as the small atomic radius of V^V is not able to stabilize the high surface negative charge of the oxo- cluster.[29,31] The calculated HOMO-LUMO gap of the hypothetical $[V^V{}_6O_{19}]^{8-}$ (3.62 eV) is significantly lower than that of the analogous heavier congener group V metal clusters ($[Nb^V{}_6O_{19}]^{8-}$ and $[Ta^V{}_6O_{19}]^{8-}$) which is ~4.9 eV.[29] Because of this, hexavandate systems are easier to reduce and thus are highly relevant for photo-redox reactions. Through substitution of the bridging μ_2-oxo ligands for capping protective groups such as organic alkoxo- or tris-alkoxo ligands, or incorporation of inorganic metal cations, the photoactive $\{V_6O_{19}\}$ clusters can be stabilized.[29–31] Alkoxohexavanadate cores are often in a mixed valence state, containing the larger V^{IV} species, increasing the HOMO-LUMO gap and stabilizing the core complex.[31] It is also possible to substitute all the bridging oxo- groups, leading to the formation of the stable neutral complex $\{V^{IV}{}_4V^V{}_2O_7(OR)_{12})\}$.[31,33]

Synthesis of mono- and di-substituted Lindqvists via conventional heating (i.e. conduction and convection) has been reported as early as 1984.[34] Monosubstituted and bi-substituted polyoxomolybdates and polyoxotungstates, represented in Figure 1.d: $\{VW_5O_{19}\}$,

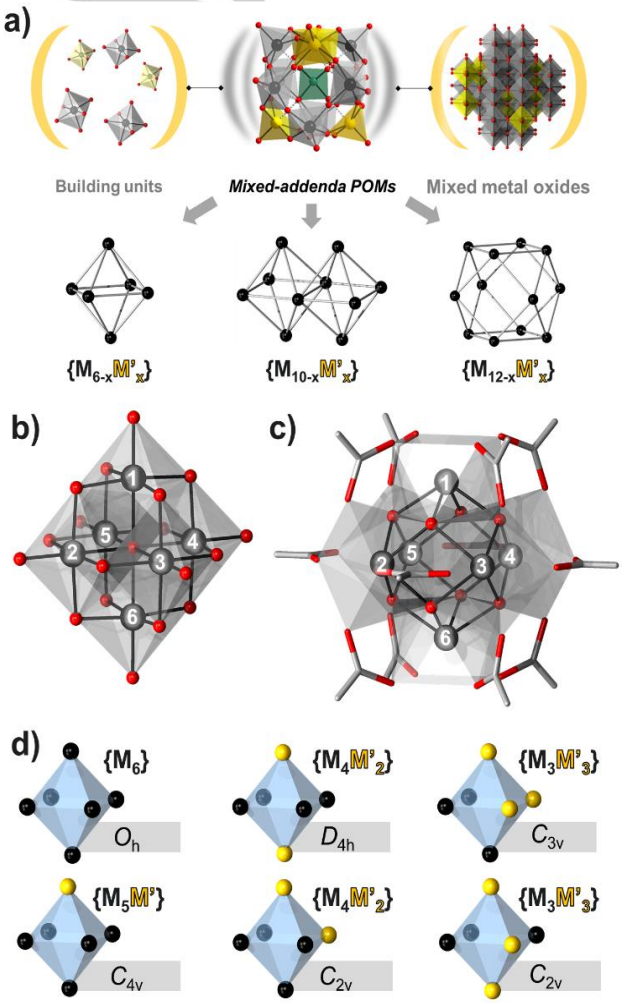

Figure 1: a) Schematic representation of the positioning of mixed-addenda POMs and their transition metal analogues between mononuclear oxometallate building units and bulk metal oxides (top row); representation of the different frameworks covered in this minireview (bottom row). b) Lindqvist type $\{M_6O_{19}\}$ polyanions; c) $\{M_6O_8L_{12}\}$ where L = RCOO$^-$ ligand. d) polyhedral representation of the different configuration when substituting the addenda centres in hexametalate structures. Colour code: M = black, O = red, and M' = yellow spheres, $\{MO_6\}$ = grey and $\{M_6\}$ = blue octahedra.

$\{VMo_5O_{19}\}$, ($\{V_2W_4O_{19}\}$, $\{V_2Mo_4O_{19}\}$, show improved photo-activity of the cluster which is increased in the presence of UV light. In addition, the photoactive window is also extended from a maximum of λ = 327 nm in the pure molybdenum cluster, up to 450 nm in the V-substituted clusters, due to the new dominating O → V LMCT transitions.[25,35] Time-dependent DFT calculations suggest that two transitions around 399 nm are due to mixed O → V and O → Mo transitions within the visible adsorption range, explaining the increased light absorption range of the mixed-addenda form.[25] The excited state configurations, as calculated with spin-restricted B3LYP-ZORA-TD-DFT are displayed in Figure 2.a.

Synthetically, the formal substitution of metal addenda within the mixed-metal Lindqvist clusters is challenging to control and to accurately characterize, since all metal positions are thermodynamically equivalent thus resulting in the formation of several configurational isomers (Figure 1.d).[25,36] Using high-resolution electrospray ionization mass-spectrometry (HR-ESI-MS), purity of a single heterometal species can be confirmed, and single crystal X-ray diffraction is used to determine the position of the metals. However, the later technique comes with a drawback on the resolution of the individual metal positions especially when the metals have similar scattering factors. Nuclear magnetic resonance (e.g. ^{51}V and ^{183}W) often provide insights whether single or multiple mixed-addenda POM configomers are present in solution or within the purified product.[25,36]

The use of microwave directed synthesis by Karoui and Ritchie led to the first characterization of the tri-substituted $[V_3Mo_3O_{16}((CH_2O)_3CCH_3)]^{2-}$ in 2017, which requires stabilisation by organic moieties.[37,38] These three substitution patterns: {1,2,3}, {2,3,6}, {2,3,4} and {2.3.5} are displayed in Figure 2.b. The fast and efficient energy transfer of a microwave-based system promotes the formation of $\{V_3Mo_3\}$ clusters which were previously unreachable through conventional heating. Single crystal X-ray structure of these trisalkoxide functionalized clusters stabilized with TBA counterions, reveal the formation of three distinct structural isomers, where each metal site has a certain occupancy of Mo and V. Although X-ray diffraction shows an averaged image, the isomer group can be identified through length of M−O bonds present.[36] Using DFT, the possible isomers of the $\{V_3Mo_3\}$ cluster were identified. The most favourable positions for vanadium to occupy were found to be facial positions and in the two less favourable isomers, only a single vanadium ion occupied a meridional position.[37] The energy difference between the structure where three vanadium atoms are present in the favourable facial position {1,2,3,} and those having two adjacent vanadium ions in the facial and a single one in the middle meridional position ({2,3,5} and {2,3,6}) is only +7.7 kJ·mol^{-1}, explaining why all three isomers are present in the synthesis product, although {1,2,3} is the most stable isomer. Other isomers of this system are not experimentally accessible due to their high relative energies. As well as stabilizing the structure, the presence of organic ligands contributes to isomers determination through ^{1}H-NMR analysis of the deshielded protons. For example, in $[V_3Mo_3O_{19}((CH_2)_3CCH_3)]^{2-}$, the number and chemical shift of methylene resonances are directly influenced by the position of electron deficient Mo^{VI} and/or V^V species. In this case, the C_{3v} {1,2,3} isomer was identified through a single methylene peak, whereas the C_s {2,3,6} form showed two broad doublets and a singlet.[36,37] Of interest is also the structural isomerism displayed by the increased nuclearity of vanadium substituted polyoxomolybdates and polyoxotungstates.[25,35,39]

Considering the stark changes in electronic structure,[40] single metal substitutions within the Lindqvist hexametalate can be considered the most common and reported types of substitutions. Depending on the coordination affinity and environment of the substituting heterometal, monomeric or dimeric (i.e. sandwich-like) assemblies can occur. Sandwich can involve two monosubsituted Lindqvist POMs such as the dimeric $[Cr_2(OH)_4Nb_{10}O_{30}]^{8-}$ assembly.[41] Alternatively, sandwich structures can be constructed also when one substituting metal centre (typically a lanthanide) is shared between two lacunary Lindqvist POMs. An example for the later may be the $[Ho(W_5O_{18})_2]^{9-}$ polyanion that shows potential as a quantum bit (qubit).[42] Many different heterometal substituents may provide functionalization with organic moieties, effectively altering the electronic, chemical and modular properties of the Lindqvist units.[43–45] In recent years the formal substitution has been extended also to alkoxo stabilized vanadium hexametalates and substitutions with 3d heterometals (e.g. Fe, Ti)[46–48] has been recently highlighted as a promising strategy in designing POM-based battery systems.[49]

2.2 Modular $\{M_{6-x}M'_xO_8\}$ as MOF Subcomponents

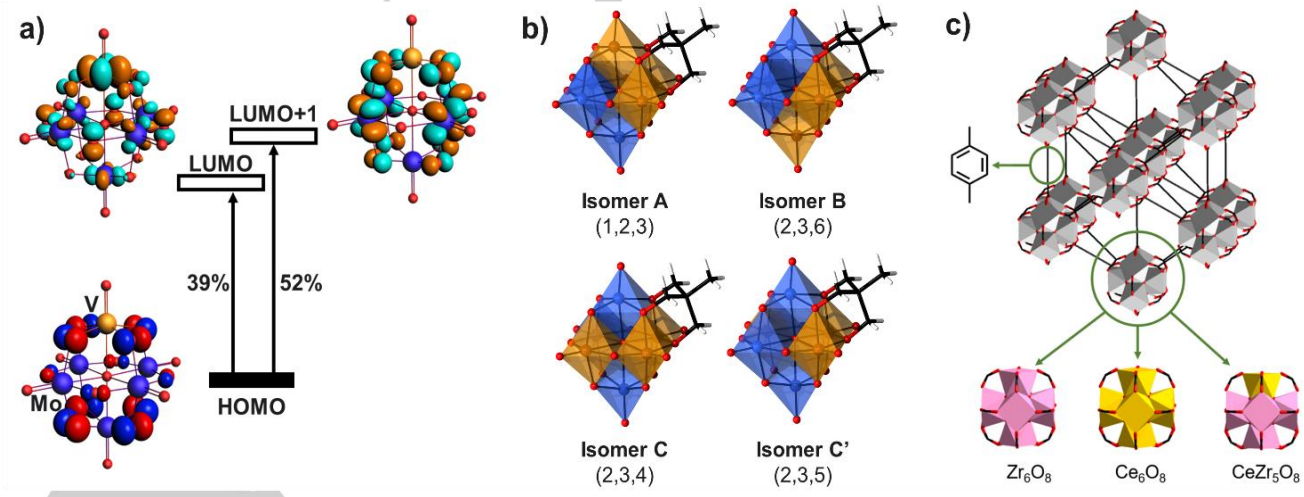

Figure 2: a) Major contributions to the first calculated excitation in $[VMo_5O_{19}]^{3-}$ as adapted from Reference [25]; b) Combined ball-and-stick and polyhedral representation of $[V_3Mo_3O_{19}((CH_2)_3CCH_3)]^{2-}$ hybrid polyanions. Isomer assignment according to Figure 1.b; c) Polyhedral representation of a fragment of MOF UiO-66 incorporating $\{M_{6-x}M'_xO_8\}$ nodes. Colour code: V = orange, Mo = blue, and O = red spheres, C = black, and H = white sticks, $\{VO_6\}$ = orange, and $\{MoO_6\}$ = blue octahedra. $\{MO_8\}$/$\{MO_8\}$ = grey, $\{ZrO_8\}$ = pink, $\{CeO_8\}$ = yellow, square antiprisms, O = red spheres. Ligands have been omitted for clarity.

Many mesoporous MOFs can be built by interlocking of organic carboxylate-terminated components with metal based coordination nodes.[50–55] MOFs exhibit many highly sought characteristics such as high terminal stability, self-assembly, large internal surface area, high crystallinity, and many other features that make them suitable for many applications, including heterogenous catalysis. Although the first 3D MOF was described in 1999 by Yaghi *et al.* and since then MOFs have received an enormous amount of interest, there is currently no strict definition as to exactly what can be classified as a MOF.[53,54] Polynuclear metal oxo clusters interconnected by rigid organic linkers can also produce extended and crystalline MOFs that remain stable even upon creation of defects and removal of guest molecules (i.e. activation by the removal of trapped solvent molecules).[53] For catalytic purposes, particular interest has been given to the use of Lewis-acidic metals such as Zr, Ce and Ti, as their catalytic activity is already well-established. Formation of hexametalic-oxo $\{M_6O_8\}$ clusters that are found in some MOF architecture, increase the accessibility and local density of Lewis acidic metals for use in catalysis.[51,56]

Furthermore, through careful selection of metals and linkers, photon collection and energy transfer can be controlled, providing highly specific catalytic systems for artificial photosynthesis and artificial enzymes.[51,57,58] Modulation of these systems, by using different organic molecules and different metal-oxo clusters has resulted in more than 20,000 different MOFs being reported so far.[59] Additionally, through use of competing modulators such as formic acid during the synthesis, reactivity of the MOFs can be increased by generating defect sites (cationic and anionic vacant sites). This increases access of the substrate to a greater number of metal centres and promotes H_2O coordination, priming the catalyst for acid-base reactions.

The $\{M_6O_8\}$ cluster is a common motif in Ti^{IV}, Zr^{IV}, Hf^{IV} and Ce^{IV}-based MOFs. One of the most documented MOFs,UiO-66 (Figure 2 c), consists of 12-coordinated $\{Zr_6O_8\}$ clusters linked by benzene dicarboxylic acid.[60] UiO-66 shows exceptional resistance to both temperature and pH, and is reusable as a heterogeneous catalyst. Its reactivity can be modulated through either substituting Zr^{IV} for another metal such as Ti^{IV} or Ce^{IV}, or though the introduction of defects into its structure during the synthesis stage.[61–63] Mixed metal MOFs, containing hybrid clusters such as $\{CeZr_5O_8\}$, $\{HfZr_5O_8\}$, and $\{TiZr_5O_8\}$ (Figure 3 c) have recently been synthesized and $\{CeZr_5O_8\}$ has been verified experimentally.[63] Considering the synthetic approach, it is generally a challenge to determine whether true formal substitution of the hexametalte cores occurs or whether the added heterometals simply graft on the hexametalate nodes (i.e. they act as MOF dopants). that is they only dope the MOF. To be able to answer this, number of complementary techniques are used (*vide infra*).

Inductively coupled optical emission spectroscopy (ICP-OES) determines the ratio of metals present within the MOFs and the use of extended X-ray adsorption far edge spectroscopy (EXAFS) is required to determine the precise position of each metal ion within the cluster. Indeed, an EXAFS study of Zr/Ce-UiO-66 revealed that the metal-oxo clusters are not purely bimetallic, but rather both monometallic and mixed-metal oxo clusters are generated within the framework.[36,64] By varying the ratio of each metal salt present within the hydrothermal synthesis reaction, a series of Zr/Ce-UiO-66 and Zr/Ce-MOF-808 was synthesised and characterised fully. When Ce^{IV} loading was less than 17%, only $\{Zr_6O_8\}$ and the mono-substituted $\{CeZr_5O_8\}$ clusters were present within the UiO-66 matrix, despite the mixed cluster being energetically less favourable than the pure metal cluster, resulting in a decrease in stability of Zr/Ce MOFs in comparison to the pure Zr_6 form of UiO-66. Above 17% of Ce, there was a distinct transition to the presence of only $\{Ce_6O_8\}$ and $\{CeZr_5O_8\}$ clusters. The three types of cluster are shown in yellow and pink in Figure 2.c, for UiO-66.

Of importance is the retention of the monometallic MOF's global structure when a second metal species is present within the cluster. This was monitored using powder X-ray diffraction (PXRD), and often small shifts in characteristic unit cell 2θ values confirmed incorporation of different sized metal species based on changes in crystal lattice unit size.[62,65] Extended X-ray adsorption fine structure spectroscopy (XAFS) confirmed that the local metal environment retained the same coordination states regardless of clusters'mono- or bi-metallic nature.

Through post-synthetic exchange, Zr/Ti bimetallic MOFs have been formed and have proved to have enhanced photocatalytic performance when compared with the mono-metallic species of Zr-UiO-66-NH_2, where, in contrast to UiO-66, the linker (2-amino terephthalic acid) is functionalised with a primary amine group.[65] The synthesis of bimetallic Zr/Ti MOF was achieved by incubating Zr-UiO-66 with $TiCl_4(THF)_2$ in DMF at 100 °C and 120 °C for 4 and 16 days respectively, to achieve maximum exchange. Indeed, when 53.4% of Zr^{IV} ions were substituted with Ti^{IV} reduction of CO_2 measured after 10 hours was 1.7 times greater (see Figure 3) compared to the pure Zr-UiO-66.[65]

Combining electron paramagnetic resonance spectroscopy (EPR) and diffuse reflectance spectroscopy (DRS) with DFT calculations, it has been shown that Ti^{IV} acts as electron mediator rather than the reactive ion within this system, increasing the efficiency of charge transfer from the excited state -NH_2 present on the 2-amino terephthalic acid linker, to the photoactive metal species.[62,66] Despite the geometry of the Zr^{IV} d^0 orbital being conformational suited to overlap with the excited LUMO of the primary amine group, the overlap is poor due to energetic differences and so formation of the excited state Zr^{III}-O-Zr^{IV} via LMCT is more limited than formation of Ti^{III}-O-Zr^{VI}.[66] Additionally, the excitation state lifetime of $\{Ti_6O_8\}$-systems is much longer than that of the $\{Zr_6O_8\}$-systems, making the $\{Ti_6O_8\}$-system more suited for catalysis.[57,66] As the electronic states of Ti^{III} and Zr^{IV} overlap, formation of the photo-reductive Ti^{IV}-O-Zr^{III} species is promoted. DFT shows the presence of additional bands in the Ti^{IV} doped UiO-66-NH_2 species as Ti^{IV} atoms contribute more to the bottom of the conduction band (LUMO) giving more favourable orbital overlap.[62,65] This was confirmed experimentally with DRS as an additional peak at 500 nm confirms amine-Ti^{IV} interactions.[62]

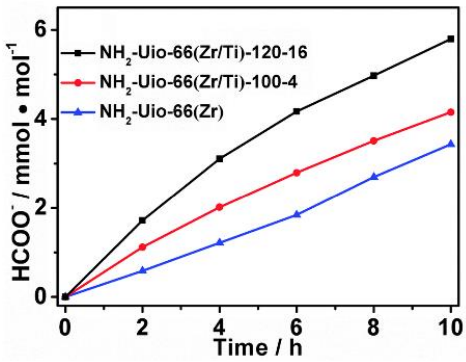

Figure 3: The increase in Co_2 reduction to $HCOO^-$ when Ti/Zr-UiO-66 is present, compared to Zr-UiO-66. 100/120 refer to temperature of metal exchange reaction and 16/4 the number of days of exchange reaction. Reproduced with permissions from ref. 50 Copyright (2015), with permission from The Royal Society of Chemistry

A third synthesis method, specifically designed for synthesis of mixed-metal, mixed-oxidation state MOFs has also been successful.[67,68] This involved synthesis of the mixed metal trimeric acetate SBUs first, followed by addition of the iPrOH linker. This has allowed the synthesis of Fe/Co, Fe/Ni and Fe/Mg MIL-127, with each MOF containing a 2:1 ratio of Fe^{III}:M^{II}.[68] By incorporating these different metals, the affinity for CO adsorption was significantly altered, in line with the electronegativity of the M^{II} species present (Ni^{II}>Co^{II}>Fe^{II}>Mg^{II}).

3. Mixed-addenda decametalates

The decavandate $[V^{V}_{10}O_{28}]^{6-}$ and its related $[Nb^{V}_{10}O_{28}]^{6-}$ derivative are one of the most stable polyoxovanadates[30] and polyoxoniobates[69] in aqueous media and its crystal structure has been known since 1966.[70] Over the past decades, Nb^{V}- and Ta^{V}-based analogues have been reported,[71–73] while the formation of Mo^{VI} and W^{VI} based analogues is unknown.[74] To date, the configurations adopted by substitution of the ten metal sites has not been systematically explored. However, for general discussion, we note that it is well-established that the particular decametalate system exhibits three groups of inequivalent sites (see Figure 4.a). In sites A and B (in total 8 addenda centres), the mixed addenda centres adopt terminal metal-oxo bonds, while in the other site (site C), two addenda centres do not. Following the different affinities for heterometals to stabilize terminal metal oxo bonds, there are different affinities for particular metals to substitute sites.[75]

The metal-substituted decavanadate $[H_2Pt^{IV}V_9O_{28}]^{5-}$ exists in only one configurational isomer, with the substituted Pt^{IV} adopting one of the two central C sites surrounded by bridging oxo-ligands (Figure 4.b).[76] This structure was determined using single crystal X-ray analysis, and was further confirmed via ^{51}V and ^{195}Pt NMR. [76,77] In some systems of low symmetry, DFT calculations are required to support structural determination from heteronuclear NMR due to low sensitivities of the NMR responsive isotopes and large chemical shift anisotropy (especially for ^{183}W and ^{195}Pt).[78] This problem was addressed by Vankova and co-workers who developed corrections to DFT for modelling the expected POM NMR spectra. The same substitution pattern was seen in the Fe and Ni substituted decaniobates $[H_2Fe^{III}Nb_9O_{28}]^{6-}$ and $[H_2Ni^{II}Nb_9O_{28}]^{6-}$,[79] and in the Ti substituted $[TiNb_9O_{28}]^{7-}$.[41] Additionally, this positioning was also observed in the larger d-block metal substituted $[MnV_{14}O_40]^{7-}$ anion that contains a central $\{MnO_6\}$ octahedron, surrounded by 14 structurally distorted $\{VO_6\}$ octahedra.[80]

The substitution of addenda centres in $[V^{V}_{10}O_{28}]^{6-}$ by Mo^{VI} has been explored as early as in the 1980s. In contrast to Pt^{IV}, Ni^{II} and Fe^{III} substitution, Mo^{VI} does not occupy the central (4, 7) (site C) position, but is located equally over the {1, 2, 9, 10} (site A) positions (Figure 4.c) in a mono-substituted $[H_2MoV_9O_{28}]$ system.[37,81] Furthermore, this system can be di-substituted, yielding two isomers of $[Mo_2V_8O_{28}]^{4-}$ represented in Figure 4.d. The isomers reported by Howarth were the *syn*- isomer with mixed addenda at {1,2} and the *anti*- with the mixed addenda at {1, 10} and were present in a 9:11 ratio respectively.[82] These isomers were found to be chemically inert and the chemical shifts of ^{51}V were unaffected by mono or di-substitution by Mo. The same substitution pattern has been observed in Nyman-Ohlin derivative Ti^{IV} substituted niobite derivative $[Nb_8Ti_2O_{28}]^{8-}$.[41,83]

Using microwave assisted synthesis, Ritchie and co-workers achieved a tri-substituted $[Mo_3V_7O_{28}]^{3-}$ system, with the four lowest energy isomers being depicted in Figure 4.e.[37] The quantum chemical calculations determined that the difference in relative energies between the most stable isomer, {1,2,9} where all Mo are in capping (site A) positions and least stable isomer {1,2,3} to be only 3.7 kJ·mol^{-1}, explaining the presence of all four isomers in the crystallographic data. For all the isomers calculated, two Mo are preferentially incorporated at sites {1,2,9 or 10} with the third Mo being located at {3,5,6 or 8} (site B), however from crystallographic analysis,

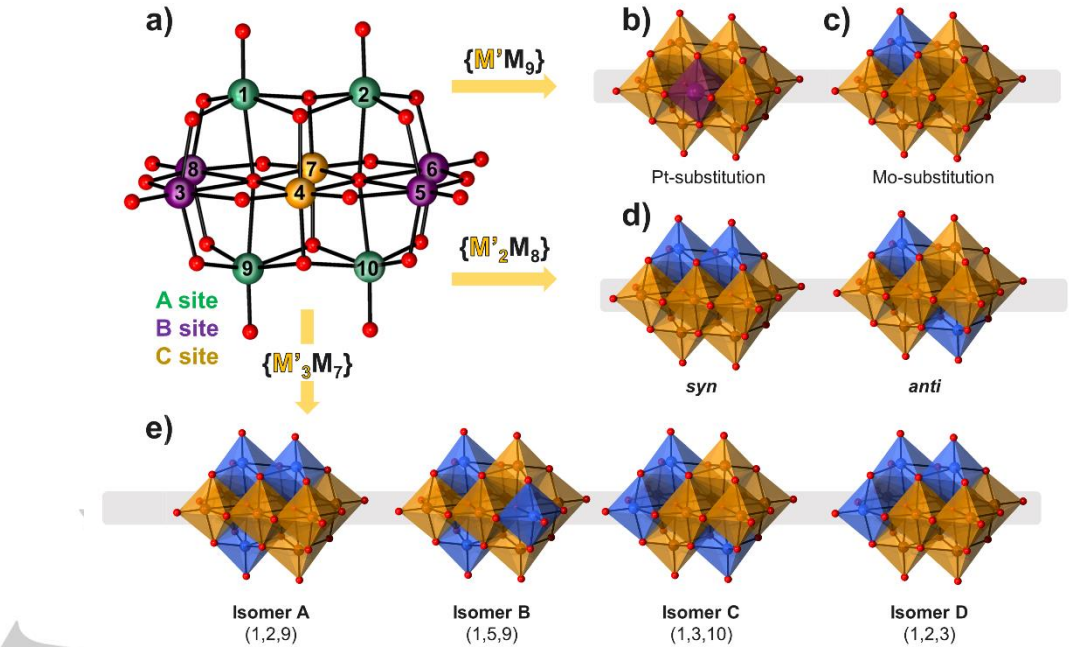

Figure 4: Combined polyhedral and ball-and-stick representation of a) $[V_{10}O_{28}]^{6-}$ together with proposed numerical assignment of the V-centres; b) $[H_2Pt^{IV}V_9O_{28}]^{5-}$; c) $[MoV_9O_{28}]^{5-}$; *syn*-/*anti*-$[Mo_2V_8O_{28}]^{4-}$; $[Mo_3V_7O_{28}]^{3-}$ isomers presented following the proposed numerical assignment. Colour code: V = orange, Pt = purple, Mo = blue, and O = red spheres, $\{VO_6\}$ = orange, $\{PtO_6\}$ = purple, and $\{MoO_6\}$ = blue octahedra. Protons have been omitted for clarity.

the exact location of the third Mo could not be identified, and thus DFT calculations based on the four isomers (Figure 4.e) were required to provide additional insight.

Advances in the decaniobate system have been made as well. The decaniobate systems have been successfully substituted with a variety of 3d cations Examples are the $[H_2Fe^{III}Nb_9O_{28}]^{6-}$ and $[H_3Ni^{II}Nb_9O_{28}]^{6-}$

4. Mixed-addenda Dodecametalates

The crystallographic elucidation of dodecametalates was pioneered during the early 1930's when James Fargher Keggin reported the structure of the 12-tunstophosphic acid.[12,13,84] This structure rapidly proved to be common among many other dodecametalates and became widely known as the Keggin structure. From a modern perspective, the Keggin structure can be described as a "host-guest" clathrate system, where a central $\{XO_4\}$ tetrahedral group is encapsulated by a cuboctahedral and neutral metal-oxo cage with formula $\{M_{12}O_{36}\}$ (Figure 5 upper left).[18] The clathrate-like model is often in alignment with the pronounced ionic bonding between the guest anions and the shell.[85,86] When virtually removing the central $\{XO_4\}$ unit and the twelve terminal oxo ligands of the Kegginoidal (i.e. Kegging-like) $\{M_{12}O_{36}\}$ structure, one derives a $\{M_{12}O_{24}\}$ (Figure 5 upper central) skeleton which is common among many late transition metal oxometalates.[13,18] In that regard the elusive $\{M_{12}O_{24}\}$ structure is viewed as a plenary and saturated topology with an ideal O_h symmetry point group that is comprised of twelve corner-sharing $\{MO_4\}$ square planes. In this topology, the twenty-four μ_2-O centers define corners of a virtual rhombicuboctahedron. The rhombicuboctahedron exhibits eighteen square faces that are covered by {M} centers of {MO} units in $\{M_{12}O_{24}\}$ and $\{M_{12}O_{36}\}$ respectively.[13] In that regard the overall Kegginoidal structure can accommodate up to additional six {M} centers of {MO} units leading to $\{M_{18}O_{24}\}$ or $\{M_{18}O_{42}\}$ archetypes that are representative for late transition isoPOMs (e.g. $[Pd_{18}O_{24}]^{12-}$) and polyoxovanadates (e.g. $[V_{18}O_{42}]^{12-}$).[13] Further on, $\{M_{12}O_{24}\}$ represent a fragment of metal-oxo bronzes and can be structurally transformed to an "open" topology which with the stabilization of trigonal $\{XO_3\}$ or tetrahedral $\{XO_4\}$ groups (L) can lead to the formation of cuboidal systems $\{M_{12}O_8L_8\}$ where M = Cu, Pd, Au or Mn.[18,87] The three different systems share similar virtual cuboctahedral metal addenda network which is subject to substitutions. Substitution of metal addenda with other heterometals is common among the classical Keggin systems and the POM cuboids. This normally leads to only minor and gradual changes in the geometry and the bonding energy, often allowing multiple structures to co-form during synthesis when simple precursor materials are used (see section 3.1. for details).

On the other hand, among the 18-metalate archetypes, the isopolyoxovanadate archetype $\{V_{18}O_{42}\}$ can undergo addenda metal substitution with bulky handle-like heterogroups of the type E-O-E where E = As, Sb or R-E'-O-E'-R where E'/R = Si/O, Ge/O and Ge/S.[88] Owing to the bulkiness of the substituting units, these structures can exhibit significant internal strains which affects their overall bonding energy and polyanion shape.[89] Eventually, the bulkiness introduces more severe energetic discrepancy among different configomers which renders only few substituting topologies stable enough to be isolated.[90] Although heterogroup substituted polyoxovanadates are not part of this review, they have been extensively reviewed in recent articles by Streb,[91] Monakhov and coworkers.[88] In addition, we note that particular substituting

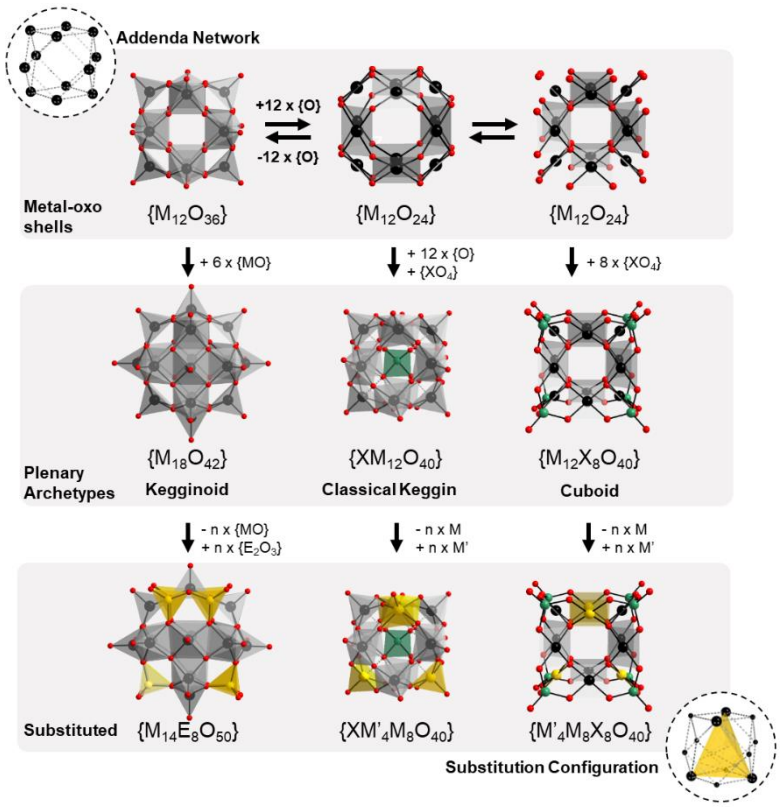

Figure 5: Schematic representation of three different addenda substituting systems that can be seen to derive from classical Kegginoidal systems. Despite the obvious differences, all systems can exhibit configurational isomerism that closely resembles substitution in a cuboctahedral systems. Color code: M = black, O = red, X = green, substituting M or $\{E_2O_3\}$ groups = yellow, $\{MO_4\}$/$\{MO_5\}$ = yellow for substituting, grey planes/polyhedra for all remaining.

configurations can be common among the different archetypes, one of them being the four-addenda center substitution in a tetrahedral fashion scenario (Figure 5, bottom row).

4.1 Mixed-addenda Kegginoids and their applications

The first substitutions of the addenda centers was achieved during the late 1950's and early 1960's when different tungstocobaltates were under investigation.[11] By 1966, Baker and coworkers established that many different mixed-addenda heteropolyanions with the general formula $[(XO_4)M_xM_{12-x}O_{36}]^{n-}$ can be formed.[92] By reaction of tungstate and vanadate precursors in aqueous media, Pope and coworkers in 1973 showcased that mixed-addenda $[(XO_4)V_xW_{12-x}O_{36}]^{n-}$ polyanions can be formed.[93] The existence of different isomeric species was established based on the observation of multiple ^{31}P NMR chemical shifts that could be traced to the encapsulation of phosphate groups in different configurations of mixed metal-oxo shell environments. From these studies, Pope and coworkers came to the original idea that different positional, or what one may call nowadays configurational isomers, may be forming. In 1975 Scully and Pope enumerated and reported the unique isomer sets existing for the α-$[(XO_4)M_xM_{12-x}O_{36}]^{n-}$ structure.[94] Later on in his book *Hetero and Isopoly Oxometalates*, Pope also reported the number of enumerated isomers for the *β*-$[(XO_4)M_xM_{12-x}O_{36}]^{n-}$ structure (see Figure 6.a),[17] however without an actual report on the existing configuration sets.

Considering the overall improved stability of the fully oxidized *α*-Keggin systems versus the *β*-Keggin,[86] most metal substituted POM systems are also *α*-Keggin in character.[34,95–100] Whenever multiple configurational isomers form, there is a possibility for rearrangement in solution. This is the case because many of the monolacunary α-$\{XM'_{11}O_{39}\}$ polyanions and their monosubstituted α-$\{XMM'_{11}O_{40}\}$ derivatives are thermodynamically more stable compared to the respective $\beta_{1\text{-}3}$ configurations (Figure 5 b).[101] An example is the mixed-metal polyanion $[Al(AlOH_2)W_{11}O_{39}]^{6-}$ which in solution readily forms $\beta_{1\text{-}3}$ isomers as kinetic products, however upon prolonged heating in aqueous media (25 days at 100°C), these isomeric mixtures turn purely to α-isomers based on ^{27}Al NMR.[102]

On the other hand, detailed ^{31}P and ^{51}V NMR studies of $[PV_2Mo_{10}O_{40}]^{5-}$ have indicated that five different isomers (counting enantiomers as a single isomers) form in solution (Figure 5 c), while there is only a minor contribution of *β*-Keggin substituted configurations.[26,103,104] These isomers are very similar in energy, deviating within ca. 8.4 kJ·mol^{-1}.[105] However the difference in the relative energies can increase up to 41.8 kJ·mol^{-1} when comparing the most stable configuration with the least stable configuration of tungsto-titanate analogs α–$[PTi_2W_{10}O_{40}]^{7-}$.[106] The later isomers exhibit configuration stability trends in the order from most stable to least stable isomer {1,4} > {1,5} > {1,11} > {1,2} > {1,6} (numbering from Figure 6.c).

4.1.1 Coordination modes from oligomers to extended solids

Besides the structural and isomeric problem that is common among mixed-metal Kegginoids, the substitution type can also influence formation dynamics and solution properties of the formed isomers. Formation dynamics are affected by size, charge, and the covalent compatibility of the heterometallic groups that substitute the addenda centers in the original Keggin matrix (predominantly *α*-Keggin but also *β*-Keggin). Depending on the preparation method, single or multiple isomers can co-form in solution. On the one hand, how these

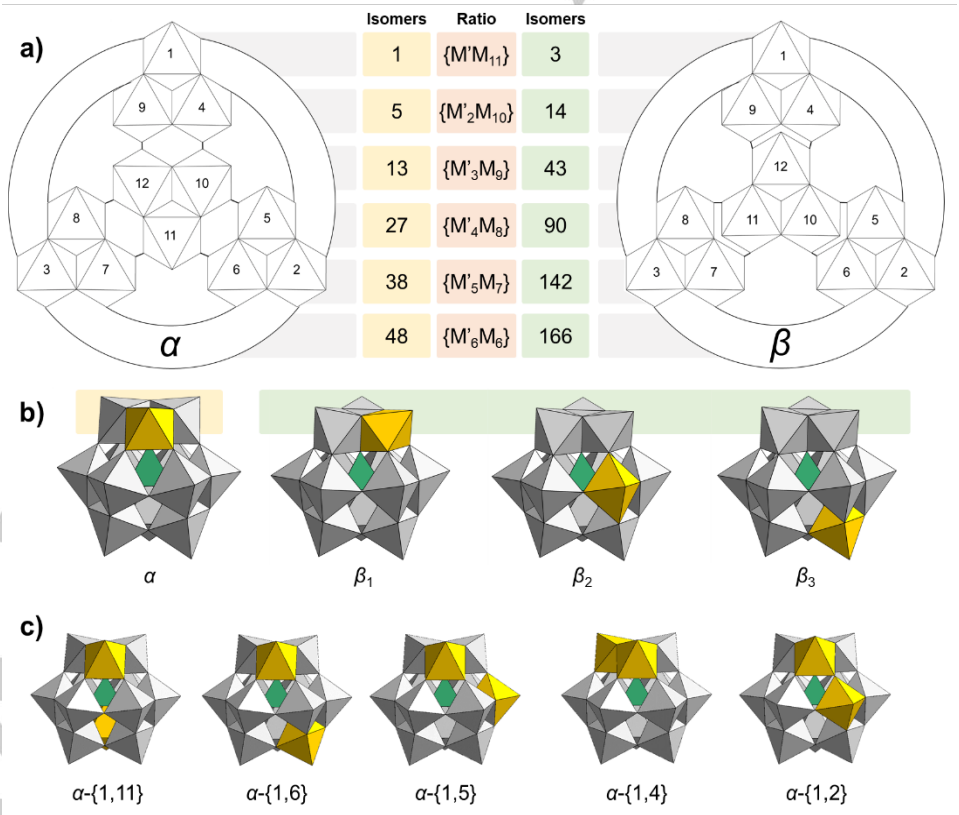

Figure 6: a) Open projection and graphical representation of the connectivity between different triads in the α-Keggin and β-Keggin structure. The specific positions of each individual polyhedral is enumerated following the IUPAC recommendations.[140] b) Three different $\{XMM'_{11}O_{40}\}$ isomers. c) Five different $\{XM_2M'_{10}O_{40}\}$ configomers. Color code: $\{XO_4\}$ = green tetrahedral, $\{MO_6\}/\{M'O_6\}$ = yellow/grey octahedral respectively.

structures covalently interact in solution is dominated by the terminal oxo, hydroxo or aqua ligands attached to the substituting ligand. Substitution with a lanthanide cation often leads to formation of large and elusive coordination spheres, which with the aid of oxo or hydroxo ligands can further agglomerate into large lanthanide functionalized POM structures.[107] On the other hand, many *d*-block substituted POMs typically exhibit a single terminal oxo/hydroxo or aqua ligand per metal center. Depending on the bonding between the substituting metal center and the adjacent terminal moiety, further dimerization or oligomerisations can be realized.[108]

Mixed-metal Kegginoids with classical addenda centers in high oxidation states (e.g. V, Mo, W) can form strong terminal oxo bonds. The process of protonation of the terminal oxo followed by POM dimerization and subsequent hydrolysis has been calculated as highly endothermic process and thus dimerization in acidic media is not promoted for those systems.[108,109] However, the lower oxidation state hetero addenda centers such as titanium(IV) or niobium(V) also show high affinity for initial protonation due to the higher nucleophilicity of the lower charged heterometal region. Generation of the M−$(OH)_2$−M intermediate is exothermic, followed by loss of water.

In that context, the dimeric structure usually is lower in energy than the monomeric form, as shown by calculations performed by López *et al*.[108] For the Ti−O−Ti bridged $\{TiPW_{11}O_{40}\}^{5-}$ Keggin, this results in a reduction of 197 kJ·mol^{-1} , while for the $\{NbSiW_{11}O_{40}\}^{5-}$ Keggin, with Nb−O−Nb bridges, the reduction in energy is closer to 105-126 kJ·mol^{-1}.[108] Such constructions can be of interest for the oxo linked systems. Further protonation can occur around the substituting site, leading to Brønsted acid catalysis.[110] This allows for intermolecular proton transfer and formation of the active hydroperoxotitanium (IV) species, resulting in enhancement of the catalytic activity of the complex-catalytic epoxidation of alkenes with H_2O_2.[110]

The simplest example of dimerization is presented by the condensation of two monosubsituted POMs of the α-$\{XM'M_{11}O_{40}\}$ Keggin type into $\{(XM_{11}O_{39}M')_2O\}$, represented in Figure 7.a. Considering that these bulky POM units are solely connected via a single oxo/hydroxo center, they can undergo significant conformational changes in solution. One can derive such conclusions when comparing the substituted Kegginoids $[(PTiW_{11}O_{39})_2O]^{8-}$ and [α-$SiW_{11}O_{39}Ru^{III}(H_2O)]^{5-}$.[110,111] Reactions of Ti^{IV} salts with monolacunary α-$[PW_{11}O_{39}]^{7-}$ polyanions also leads to dimer formation.[110,112] Mono-substituted α–Keggin [α–$SiW_{11}O_{39}Ru^{III}(H_2O)]^{5-}$ dimerizes in alkaline (pH 8) aqueous medium through formation of bridging Rh^{IV}−O−Rh^{IV} bonds.[111] The initial deprotonation of the terminal Rh−OH, is followed by formation of a Ru^{III}−O−Ru^{III} bridge, which is then oxidized in two steps to form the final Ru^{IV}−O−Ru^{IV} bridged species: [{α-$SiW_{11}O_{39}Ru^{III}\}_2O]^{12-}$.

The position of the hetero-addenda octahedra dictates the type of observed oligomerization. In di-substituted systems where the titanium octahedra are not spatially close {1,5}, but separated by four bonds (Ti-O-W-O-Ti) within each monomer, di-oxo bridged tetrameric pinwheels are formed. This was shown experimentally by Kortz *et al.* for four Kegginoidal α–(1,5) $\{Ti_2SiW_{10}O_{39}\}$ monomers (see Figure 7. b).[111,113] The addition of $TiO(SO_4)$ to an aqueous solution of the dilacunary [γ-$SiW_{10}O_{36}]^{8-}$ results in the tetrameric structure of $[\{\beta\text{–}Ti_2SiW_{10}O_{39}\}_4]^{24-}$ shown in Figure 8.b. The positions of the titanium octahedra prevent formation of the aforementioned dimers, but instead support wheel stacking and subsequent nanotube formation. When the $\{TiO_6\}$ octahedra are adjacent {1,2}, dimers are formed.

Indeed, it has been found that by varying pD, dimerization and number of bridging bonds can be controlled (Figure 7 c).[114] Addition of DCl to two equivalents of the lacunary Keggin A-α–$[SiNb_3W_9O_{40}]^{7-}$ promotes stepwise condensation, forming mono-, di- and then tri-oxo bridges between adjacent $\{NbO_6\}$ octahedra, which can then be hydrolyzed in

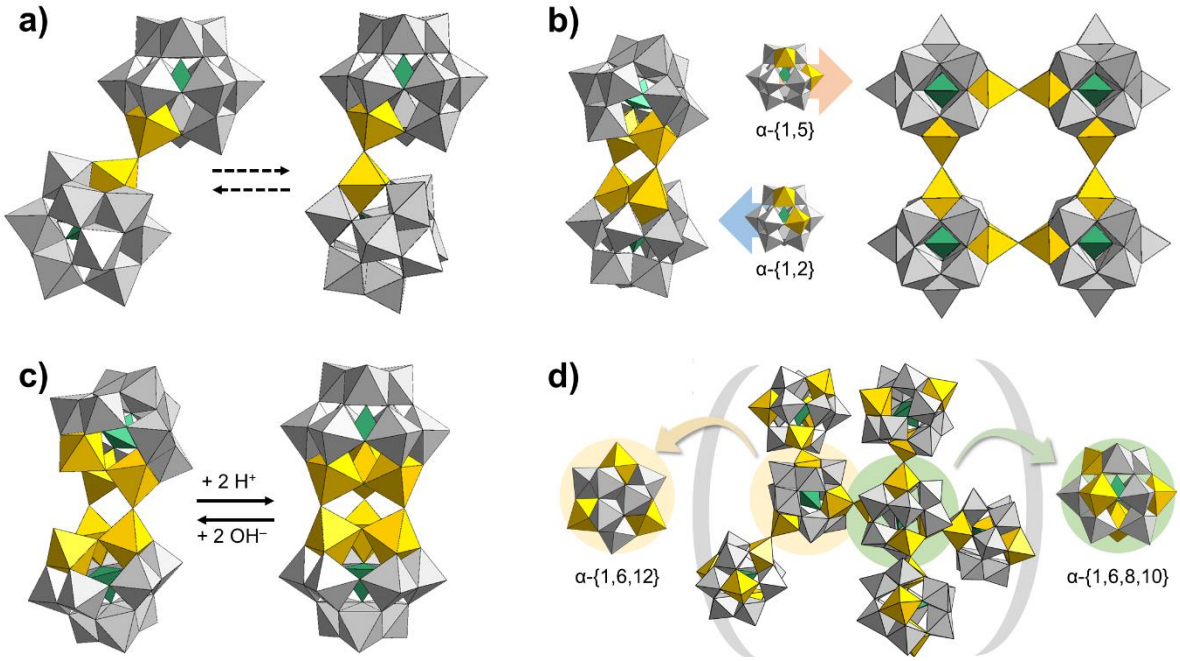

Figure 6: Polyhedral representation of different covalent interactions between mixed-addenda α-Keggin structures $\{XM_xM'_{12-x}O_{40}\}$. a) Two possible conformational isomers formed by $\{XMM'_{11}O_{40}\}$ dimers. b) Different configurational possibilities controlling the oligomerization of $\{XM_2M'_{10}O_{40}\}$ isomers, leading to either a simple dimer (left) or a tetrameric pinwheel (right); c) pH dependent dynamic covalent interactions between two (1,2,3)-substituted $\{XM_3M'_9O_{40}\}$ units. d) Extended all-inorganic networks constructed by combination of "trigonal" $\{XM_3M'_9O_{40}\}$ and "tetrahedral" $\{XM_4M'_8O_{40}\}$ units.M shown in grey, M' in yellow, central tetrahedra in green.

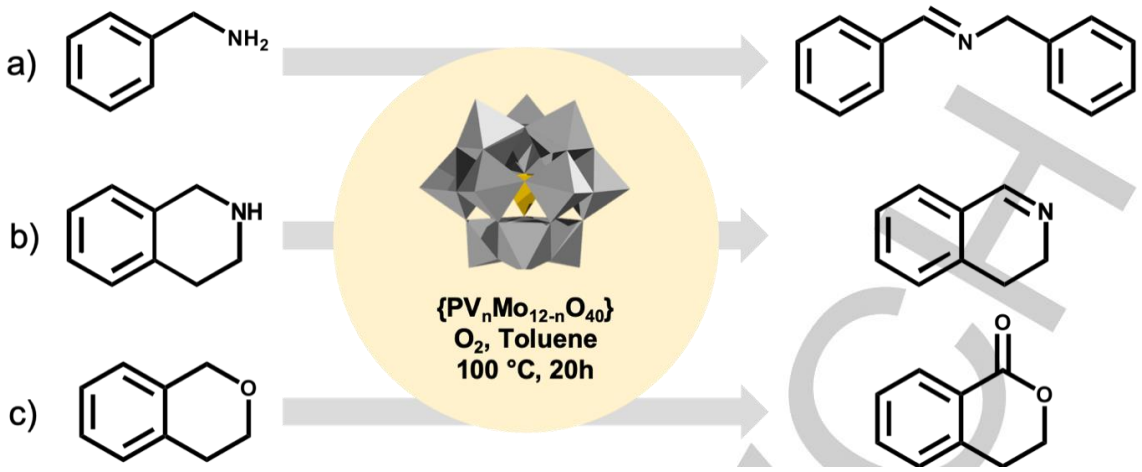

Figure 8: Reactions catalyzed by $\{PV_nMo_{12-n}O_{40}\}$ Keggin clusters with the same reaction conditions. a) Oxidation of benzylamine to N-Benzyl-1-phenylmethanimine with $H_4PVMo_{11}O_{40}{\cdot}34\ H_2O$. b) Oxidative dehydrogenation of 1,2,3,4-Tetrahydroisoquinoline to 3,4-Dihydroisoquinoline with $Na_5PV_2Mo_{10}O_{40}$ c) Oxidation of isochroman to 3,4-dihydroisocoumarin with $N[PV_6Mo_6O_{40}]$.

reverse steps through the addition of LiOH. Di-oxo bridged dimers have also been reported when Mn^{II} is introduced to the lacunary Keggin $[B\text{-}\alpha\text{-}PW_9O_{34}]^{9-}$, resulting in the $\alpha\text{-}[PMnW_{11}O_{40}]$ polyanion.[115] Dimeric $(MnPW_{11}O_{39})_2^{10-}$ structures, based on conformational isomerism of the monomer are formed. The *syn*-isomer (with both Mn on the same side) has Mn−O−Mn and W−O−W bridges, and the *anti*-isomer (Mn on opposing sides) contains mixed W−O−Mn bridges.

This suggests that it could be possible to build up extended networks of mixed-addenda Keggins through μ_2-oxo bridges based on the characteristics of the metal octahedra at each position (Figure 7.d). When Mn^{II} was added to the divacant lacunary $\gamma\text{-}[SiW_{10}O_{36}]^{8-}$, two mixed addenda configurations were formed: $\{SiMn_{1.5}W_{10.5}O_{37}\}$ and $\{SiMn_2W_{11}O_{38}\}$, each present in a 4:3 ratio.[116] These crystalize into an infinite 3D network without the need for additional linker molecules (Figure 7.d). The tri-connected $\{SiMn_{1.5}W_{10.5}O_{37}\}$ bind as trigonal nodes with the mixed addenda atoms present at positions {1,6,12} and the tetra-connected $\{SiMn_2W_{11}O_{38}\}$, with mixed addenda atoms at {1,6,8,10} bind as tetrahedral nodes, with nodes being joined through W−O−Mn bridging cross-links. This framework can be dissolved in hot water, and afterwards it reassembles into the same network.

4.1.2 Catalytic activity of mixed addenda systems

The mixed addenda Kegginoidal systems $\{PV_nMo_{12-n}O_{40}\}$, where n > 1, are able to act as oxidation catalysts for a wide range of substrates in the presence of H_2O_2 and molecular oxygen.[117–120] The use of phosphovanadomolybdates as a standalone catalyst for alcohol and phenol oxidation, carbon-carbon bond cleavage, dioxygen activation electron transfer, and other reactions was recently covered in depth by Weinstock, Schreiber and Neumann.[117]

Incorporation of a V^V/V^{IV} reversible couple in a Kegginoidal system that is able to cycle at low pH and room temperature is the key to reactivity of the systems, making these catalysts more efficient than when only $\{Mo_{12}\}$ clusters are present. $\{PV_3Mo_9O_{40}\}^{6-}$ forms adipic acid and the related dimethyl ester from 2-hydroxycyclohexanone at room temperature within 5 hours, accompanied by a colour change from orange to blue-green to brown-orange, confirming the roll of the redox active V^V/V^{IV} couple.[121,122] The same colour change is observed with the oxidation of cellulose by the $\{PV^V_2Mo_{10}O_{40}\}$ cluster.[123] Using cyclic voltammetry (CV), it was confirmed that vanadium is reduced first, and the cluster oxidation occurred in two steps: $H_8PV^{IV}_2Mo^{V}Mo^{VI}_9O_{40} \rightarrow H_7PV^{IV}_2Mo^{VI}_{10}O_{40} \rightarrow H_5PV^{V}_2Mo_{10}O_{40}$. In this cluster, the two $\{VO_6\}$ octahedra are located in adjacent $\{M_3O_{13}\}$ triads and connected through a corner shared oxygen.

A selection of published reactions is represented in Figure 8. $H_4PVMo_{11}O_{40}$ gives a 60% oxidation of benzylamine to the associated Schiff-base imine within 20h in toluene at 100 °C, compared to just 14% with the unsubstituted $H_4PMo_{12}O_{40}$ catalyst (Figure 8.a).[118] $H_4PV_2Mo_{10}O_{40}$, under the same reaction conditions also achieved high yields during oxidative dehydrogenation of a selection of benzylic amines (Figure 8.b) and $NPV_6Mo_6O_{40}$ oxidises isochroman, giving 3,4-dihydroisocoumarin selectively (Figure 8.c), again with high conversion rates.

Elucidation of the mechanism of aerobic oxidative dehydrogenation reactions was achieved with the {1,2} $PV_2Mo_{10}O_{40}$ Keggin as catalyst by Neumann and Levin using the conversion of α-terpinene to *p*-cymene.[117,124] Protonation of the V-O-V bridge between two metal centres is an essential step, providing the hydrogen atoms for the final dehydration step. Using ESR, the redox couple V^V/V^{IV} was observed, suggesting that for this reaction to occur, vanadium octahedra must be adjacent, and corner sharing. In V-O-M-O-V containing isomers, such as the {1,6} $PV_2Mo_{10}O_{40}$ where the vanadium ions are non-adjacent, electrons are not able to shuttle rapidly between the vanadium ions. [124,125] As the reduction of molecular oxygen requires two electrons, adjacent vanadium octahedral are required within the O_2 coordination site. Indeed, it has been shown through experimental and computational methods that protonation of bridging oxygen species preferentially occurs at V-O-V bridges in isomers such as the {1,2} $PV_2Mo_{10}O_{40}$ (compared to V-O-Mo) due to higher electron density.[124,126]

As well as vanadium, titanium has also been investigated as a redox active metal substitution since $Ti^{IV}O_2$ is a well-known photo-catalyst. This field is less developed due to the difficulty in synthesizing a monomeric species, although $[PTi_2W_{10}O_{40}]^{7-}$ has been reported.[113,127] Unlike with the previous vanadium substituted example, the $\{TiO_6\}$ are not in direct contact but are in adjacent triads located at {1,5}.

4.1.3 Energy Storing Materials

Through substitution of addenda atoms, the basicity and redox properties of POMs can be modulated. For example, substitution of W for Mo, forming the mixed addenda $[SiW_9Mo_3O_{40}]^{4-}$ species lowers the energy of the LUMO by 0.3 eV (from DFT calculations) without

changing the overall charge of the structure.[128] Using DFT method, it was found that the single electron reduction of the mixed species was 0.4 eV more favorable than the $[SiW_{12}O_{40}]^{4-}$, showing the mixed species to be a more efficient oxidant. The same was seen when vanadium was substituted into the $[SiW_{12}O_{40}]^{4-}$ as the V^{V} was preferentially reduced - this was experimentally verified by Hervé et al.[129] Interestingly, substitution of neodymium had the opposite effect, forming a less efficient oxidant. The effect of substitution on redox properties was investigated through experimental and theoretical methods by Laskin et al with $PMo_xW_{12-x}O_{40}^{3-}$based systems, where *x* = 0, 1, 2, 3, 6, 9 and 12.[130] Their findings show that mono-substitution of Mo^{VI} by W^{VI} in the decatungstate substantially increased the oxidation efficiency, and that tri-substituted $\{Mo_3W_9O_{40}\}$ Keggin was found to be the strongest oxidant experimentally using cyclic voltammetry (CV). This was also confirmed theoretically due to the large relaxation energy of the tri-substituted system.

The effect of vanadium position on mixed addenda POM based battery performance has been tested using the corner-sharing $K_6[A\text{-}\alpha\text{-}PV_3W_9O_{40}]\cdot 3H_2O$, and the edge-sharing $K_6[B\text{-}\alpha\text{-}PV_3W_9O_{40}]\cdot 4H_2O$ vanadium Keggin POMs.[131] The corner sharing Keggin was proved to have good columbic efficiency and electrochemically reversible vanadium redox-chemistry in this conformation due to greater ease of oxygen protonation in this isomer.[131,132]

In a recent study by Srinivasan, Stimming *et al.*, it was found that by engineering polyoxometalate-single walled carbon nanotube (POM-SWCNT) hybrid materials, the fast and efficient redox cycling that was possible within isolated POMs could be combined with double layer capacitance, making them an ideal material for highly conductive electrodes within supercapacitors.[133,134] The use of tetrabutylammonium (i.e. TBA) salts within SWCNT-TBA-PV_2Mo_{10} prevented disassociation of the POM into the acidic aqueous electrolyte. Using CV, TBA-PV_2Mo_{10} redox cycling was confirmed and showed 39% higher specific capacitance than unmodified SWCNTs. Additionally, even after 6500 cycles, capacitance retention was 95% showing the complex to be highly stable as the system cycled between $[PV_2^{V}Mo_{10}^{VI}O_{40}]^{5-}$ and $H_{6+n}[PV_{2-n}^{V}V_n^{IV}Mo_6^{VI}Mo_4^{V}O_{40}]^{5-}$.

In contrast to the previous system, where the POM needed to remain out of solution, in redox flow batteries (RFB), were the use of POMs has also been investigated, solubility of the POM is vital.[131,135] By adjusting the counter ions, POMs can be made to be extremely soluble in a specific medium, allowing high concentrations of POM to be present, resulting in exceptionally high energy density – which is a key for the efficiency of RFBs. The mixed addenda Keggin dimer $[(SiFe_3W_9(OH)_3O_{34})_2(OH)_3]^{11-}$ is more suitable to be used within RFBs than monomer species as the three electron $Fe^{II/III}$ redox cycle has a smaller effect on the overall charge density of a larger species, making it more resilient to multiple cycles. The monomeric Lindqvist *cis*-$V_2W_4O_{19}^{4-}$ was investigated as a comparison, where both V^{V} and W^{VI} were involved in the redox chemistry, however the reduction of W^{VI} was seen to be irreversible. The fully reduced Lindqvist monomer precipitated out, unlike the fully reduced dimer that remained in solution. When used in an RFB, the coulombic efficiency of the dimer was 83%, and after 20 cycles, the electrochemical yield was 55%. This is much higher than the yield recorded for the Lindqvist monomer species which showed the coulombic efficiency of 16%.

4.2 Noble metal cuboidal systems

Cuboidal systems of the type $\{M_{12}O_8(L)_8\}$ (see Figure 9) where L may be a trigonal or tetrahedra heterogroup such as $\{PO_4\}$, $\{AsO_4\}$, $\{SeO_3\}$, $\{PO_3Ph\}$ or $\{AsO_3Ph\}$, are known to exist for Pd, Au and Mn systems.[18] Such polyanions are considered of interest for encapsulation of magnetically active *d*- or *f*-block cations and construction of quantum bits (qubits) or single ion magnets.[136] Interested in diversifying the structure of cubioids, in 2014, Izarova *et al.* reported on the mixed-metal polyoxo-noble-metalate $[NaAu_4Pd_8As_8O_{40}]^{11-}$ (Figure 9), formed of aurate and palladate square planes.[137] Based on single X-ray crystallographic analysis it was not possible to distinguish the correct position of the gold(III) and palladium(II) centers in the cuboid structure. Considering that arsenate capped aurates are stable in solution and can dimerize and

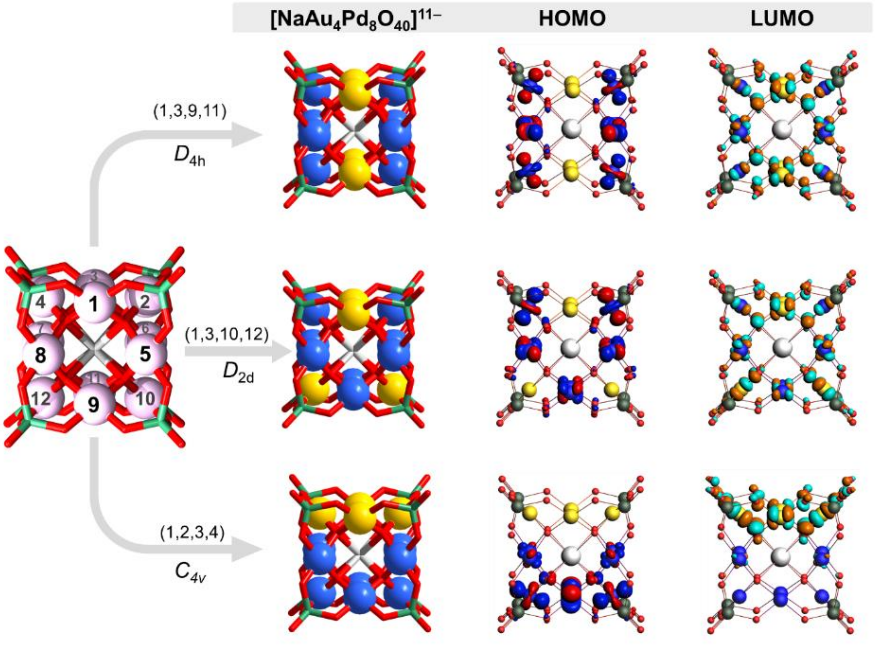

Figure 9: Schematic construction of three isomeric $[NaAu_4Pd_8As_8O_{40}]^{11-}$ cuboids by addenda substitutions in a general network (left) leading to high symmetry polyanions exhibiting different distributions of HOMO and LUMO (right). Relative bonding energy as reported using the Becke-Perdew functional. Color code: Au = yellow, Pd = blue, O = red, Na = light grey, As = green spheres/centers.

form a cuboidal-like structure, it was questionable to what degree it is possible for tetra-aurate synthons to be involved in the formation of the particular mixed-addenda cuboids. [138] Considering combinatorics, it was enumerated that eighteen configurational isomers, where only single isomer was counted per enantiomer pair can be constructed, that will cover the whole topological space. This is significantly smaller than the 27 isomers enumerated by Pope and Scully for the *α*-Keggin structure, where each enantiomer is counted separately and where the lower overall symmetry (T_d vs. O_h) contributes to the higher number of isomers. The modest set of configurational isomers allowed convenient way for DFT calculations.

Among the 18 configurational isomers, the least stable configuration was found to be the {1,2,3,4}-$[NaAu_4Pd_8As_8O_{40}]^{11-}$ structure with an overall C_{4v} point group, which exhibited tetra-aurate-like fragment.[138] The later structure was some 18 kJ·mol^{-1} higher in energy than the scenario where the four Au(III) centers occupy a virtual belt in the cuboid structure with {1,3,9,11} configuration and an overall D_{4h} symmetry point group. The later structure was found to lay only some 0.7 kJ·mol^{-1} lower in energy than the cuboidal configomer with {1,3,10,12} substitution and an overall D_{2d} point group symmetry. In this context, the DFT calculations revealed that although there was no significant change in geometric parameters, the overall bonding energy was lowered as the Au(III) centers attain positions further away from one another. In addition to this, the overall HOMO-LUMO gap energy of the studied systems enlarged with the increase in the stability. All mixed-addenda systems exhibited Pd-centred HOMO which is a qualitatively comparable scenario to polyoxopalladate systems studied at the same theoretical level.[139] On the other hand, the antibonding LUMO in the studied systems gradually transitioned from being dominantly Au-centered as in {1,2,3,4} configuration to Au/Pd-centred as in {1,3,9,11} and {1,3,10,12} configurations. This implies that as the Au-centers are closer it will be significantly easier for them to become reduced, destabilizing the overall structure, thus providing another parameter for assessing relative stability.

On the basis of frequency calculations, it was revealed that the stretching frequency of the terminal As–O bonds would be also impacted by the nature of the mixed-addenda configuration. Substituting configurations such as {1,2,3,4} give rise to two structurally inequivalent {AsO} moieties that share oxo ligands with: *i*) three Pd^{II} centers; *ii*) with two Au^{III} and one Pd^{II} center. On the other hand, highly mixed scenarios such as {1,3,9,11} and {1,3,10,12} configurations lead only to a single *ν*(As–O) stretch frequency, which was in agreement with the experimental observations.

5. Summary and Outlook

In this article we have systematically reviewed the metal substitution in several well-known plenary POMs (group V, VI and X/XI) and in their modular group IV based analogues. The formal substitution is dependent on many interdependent factors that relate to the overall stability and configuration of the mixed-addenda species, but also from the overall environment. Synthesis may be achieved via many different preparation strategies, while the identification of the formed species often requires combinations of experimental characterization strategies and theoretical studies. The properties of the mixed metal species are very attractive for applications in catalysis, energy storing materials and material science in general. Understanding of the formation of the mixed-addenda species, their speciation, abundance and control in solution, and assembly in the solid state represent important frontiers that give rise to the concept of *adaptive isomerization* in polyoxometalate chemistry. Considering the difficulties for experimental distinction between multiple isomer formations, we acknowledge that theoretical approaches are likely to provide insights and meaningful guidance for the rational material design in near future. In addition, computational insights will be of high importance to understand not only the relative stabilities but also the differences in functionalities exhibited by mixed-addenda POMs. Finally, the large but limited configurational possibilities formed by the high-symmetry mixed-addenda POM archetypes represent a very good basis for top-down study of the POM formation mechanism and solution speciation of the intermediate building block libraries which remain still an open fundamental challenge.

Acknowledgements

AK thanks Research Foundation Flanders for post-doctoral fellowship (166497/12Y9218N LV 5457). CS thanks Research Foundation Flanders for doctoral fellowship (11C9320N). All authors thank KU Leuven for research support.

Keywords: Polyoxometalate • Mixed-addenda • MOF • Catalysis • Synthesis

[1] W. H. Brock, *Norton History of Chemistry*, W.W. Norton & Co Inc, New York, NY, **1993**.
[2] R. G. Arns, *Eng. Sci. Educ. J.* **1998**, *7*, 233–240.
[3] C. S. Smith, *Science.* **1965**, *148*, 908–917.
[4] Y. Mao, T.-J. Park, S. S. Wong, *Chem. Commun.* **2005**, 5721–5735.
[5] A. J. M. Mackus, J. R. Schneider, C. MacIsaac, J. G. Baker, S. F. Bent, *Chem. Mater.* **2019**, *31*, 1142–1183.
[6] S. D. Jackson, J. S. J. Hargreaves, *Metal Oxide Catalysis*, John Wiley & Sons, Weinheim, **2009**.
[7] J. C. Védrine, *ChemSusChem* **2019**, *12*, 577–588.
[8] S. B. Ogale, T. V. Venkatesan, M. Blamire, *Functional Metal Oxides: New Science and Novel Applications*, John Wiley & Sons, Weinheim, **2013**.
[9] J. He, *Metal Oxide Varistors: From Microstructure to Macro-Characteristics*, John Wiley & Sons, Weinheim, **2019**.
[10] Z. Wang, L. Zhou, X. W. (David) Lou, *Adv. Mater.* **2012**, *24*, 1903–1911.
[11] L. C. W. Baker, D. C. Glick, *Chem. Rev.* **1998**, *98*, 3–49.
[12] R. Pütt, A. Kondinski, K. Monakhov, *Chem. Unserer Zeit* **2018**, *52*, 384–389.
[13] A. Kondinski, T. N. Parac-Vogt, *Front. Chem.* **2018**, *6*, 1–7.
[14] D.-L. Long, E. Burkholder, L. Cronin, *Chem. Soc. Rev.* **2007**, *36*, 105–121.
[15] D.-L. Long, R. Tsunashima, L. Cronin, *Angew. Chemie Int. Ed.* **2010**, *49*, 1736–1758.
[16] S. V Krivovichev, *Angew. Chemie Int. Ed.* **2014**, *53*, 654–661.
[17] M. T. Pope, *Heteropoly and Isopoly Oxometalates*, Springer Berlin Heidelberg, Berlin, Heidelberg, **1983**.
[18] A. Kondinski, K. Y. Monakhov, *Chem. - A Eur. J.* **2017**, *23*, 7841–7852.
[19] M. Nyman, P. C. Burns, *Chem. Soc. Rev.* **2012**, *41*, 7354–7367.
[20] A. V. Anyushin, A. Kondinski, T. N. Parac-Vogt, *Chem. Soc. Rev.* **2020**, *49*, 382–432.
[21] I. L. Malaestean, M. Speldrich, A. Ellern, S. G. Baca, P. Kögerler, *Dalt. Trans.* **2011**, *40*, 331–333.
[22] J. Winarta, B. Shan, S. M. Mcintyre, L. Ye, C. Wang, J. Liu, B. Mu, *Cryst. Growth Des.* **2020**, *20*, 1347–1362.
[23] A. T. Balaban, *J. Chem. Inf. Comput. Sci.* **1995**, *35*, 339–350.
[24] F. C. Hawthorne, *Acta Crystallogr. Sect. A* **1983**, *39*, 724–736.
[25] J. Tucher, Y. Wu, L. C. Nye, I. Ivanovic-Burmazovic, M. M. Khusniyarov, C. Streb, *Dalt. Trans.* **2012**, *41*, 9938–9943.
[26] A. M. Khenkin, A. Rosenberger, R. Neumann, *J. Catal.* **1999**, *182*, 82–91.
[27] C. M. Flynn, M. T. Pope, *Inorg. Chem.* **1973**, *12*, 1626–1634.
[28] M. Dabbabi, M. Boyer, *J. Inorg. Nucl. Chem.* **1976**, *38*, 1011–1014.
[29] X. F. Su, B. Zhu, C. X. Wu, L. K. Yan, Z. M. Su, *J. Theor. Comput. Chem.* **2017**, *16*, 1750054.
[30] O. Linnenberg, A. Kondinski, K. Y. Monakhov, in *Supramol. Syst. Chem. Types Appl.* (Ed.: C. Pena), Nova Science Pub Inc, **2017**, pp. 39–66.
[31] Y. Hayashi, *Coord. Chem. Rev.* **2011**, *255*, 2270–2280.
[32] R. Hoffmann, P. von R. Schleyer, H. F. Schaefer III, *Angew. Chemie*

Int. Ed. **2008**, *47*, 7164–7167.
[33] C. Daniel, H. Hartl, *J. Am. Chem. Soc.* **2005**, *127*, 13978–13987.
[34] R. I. Maksimovskaya, A. K. Il'yasova, D. U. Begalieva, D. F. Takezhanova, A. K. Akhmetova, *Bull. Acad. Sci. USSR, Div. Chem. Sci.* **1984**, *33*, 1977–1982.
[35] J. Tucher, S. Schlicht, F. Kollhoff, C. Streb, *Dalt. Trans.* **2014**, *43*, 17029–17033.
[36] H. Karoui, C. Ritchie, *New J. Chem.* **2018**, *42*, 25–28.
[37] S. Spillane, R. Sharma, A. Zavras, R. Mulder, C. A. Ohlin, L. Goerigk, R. A. J. O'Hair, C. Ritchie, *Angew. Chemie - Int. Ed.* **2017**, *56*, 8568–8572.
[38] M. Filowitz, R. K. C. Ho, W. G. Klemperer, W. Shum, *Inorg. Chem.* **1979**, *18*, 93–103.
[39] S. Herrmann, J. T. Margraf, T. Clark, C. Streb, *Chem. Commun.* **2015**, *51*, 13702–13705.
[40] M. Pascual-Borràs, X. López, A. Rodríguez-Fortea, R. J. Errington, J. M. Poblet, *Chem. Sci.* **2014**, *5*, 2031–2042.
[41] C. A. Ohlin, E. M. Villa, J. C. Fettinger, W. H. Casey, *Dalt. Trans.* **2009**, 2677–2678.
[42] M. Shiddiq, D. Komijani, Y. Duan, A. Gaita-Ariño, E. Coronado, S. Hill, *Nature* **2016**, *531*, 348–351.
[43] L. Coyle, P. S. Middleton, C. J. Murphy, W. Clegg, R. W. Harrington, R. J. Errington, *Dalt. Trans.* **2012**, *41*, 971–981.
[44] N. V Maksimchuk, I. D. Ivanchikova, G. M. Maksimov, I. V Eltsov, V. Y. Evtushok, O. A. Kholdeeva, D. Lebbie, R. J. Errington, A. Solé-Daura, J. M. Poblet, et al., *ACS Catal.* **2019**, *9*, 6262–6275.
[45] R. J. Errington, G. Harle, W. Clegg, R. W. Harrington, *Eur. J. Inorg. Chem.* **2009**, *2009*, 5240–5246.
[46] L. E. VanGelder, P. L. Forrestel, W. W. Brennessel, E. M. Matson, *Chem. Commun.* **2018**, *54*, 6839–6842.
[47] F. Li, S. H. Carpenter, R. F. Higgins, M. G. Hitt, W. W. Brennessel, M. G. Ferrier, S. K. Cary, J. S. Lezama-Pacheco, J. T. Wright, B. W. Stein, et al., *Inorg. Chem.* **2017**, *56*, 7065–7080.
[48] F. Li, L. E. VanGelder, W. W. Brennessel, E. M. Matson, *Inorg. Chem.* **2016**, *55*, 7332–7334.
[49] L. E. VanGelder, T. R. Cook, E. M. Matson, *Comments Inorg. Chem.* **2019**, *39*, 51–89.
[50] A. H. Chughtai, N. Ahmad, H. A. Younus, A. Laypkov, F. Verpoort, *Chem. Soc. Rev.* **2015**, *44*, 6804–6849.
[51] J. Lee, O. K. Farha, J. Roberts, K. A. Scheidt, S. T. Nguyen, J. T. Hupp, *Chem. Soc. Rev.* **2009**, *38*, 1450–1459.
[52] X. D. Du, X. H. Yi, P. Wang, W. Zheng, J. Deng, C. C. Wang, *Chem. Eng. J.* **2019**, *356*, 393–399.
[53] H. Li, M. Eddaoudi, M. O'Keeffe, O. M. Yaghi, *Nature* **1999**, *402*, 276–279.
[54] K. K. Gangu, S. Maddila, S. B. Mukkamala, S. B. Jonnalagadda, *Inorganica Chim. Acta* **2016**, *446*, 61–74.
[55] C. S. Diercks, M. J. Kalmutzki, N. J. Diercks, O. M. Yaghi, *ACS Cent. Sci.* **2018**, *4*, 1457–1464.
[56] S. Dan Zhao, by Zhigang Hu, E. Mahmoud Mahdi, Y. Peng, Y. Qian, B. Zhang, N. Yan, D. Yuan, J.-C. Tan, D. Zhao, et al., *J. Mater. Chem. A* **2017**, 8954.
[57] S. Yuan, J. S. Qin, H. Q. Xu, J. Su, D. Rossi, Y. Chen, L. Zhang, C. Lollar, Q. Wang, H. L. Jiang, et al., *ACS Cent. Sci.* **2018**, *4*, 105–111.
[58] A. H. Chughtai, N. Ahmad, H. A. Younus, A. Laypkov, F. Verpoort, *Chem. Soc. Rev.* **2015**, *44*, 6804–6849.
[59] H. Furukawa, K. E. Cordova, M. O'Keeffe, O. M. Yaghi, *Science.* **2013**, *341*, 6149.
[60] J. H. Cavka, S. Jakobsen, U. Olsbye, N. Guillou, C. Lamberti, S. Bordiga, K. P. Lillerud, *J. Am. Chem. Soc.* **2008**, *130*, 13850–13851.
[61] F. Vermoortele, B. Bueken, G. Le Bars, B. Van De Voorde, M. Vandichel, K. Houthoofd, A. Vimont, M. Daturi, M. Waroquier, V. Van Speybroeck, et al., *J. Am. Chem. Soc.* **2013**, *135*, 11465–11468.
[62] A. Santiago Portillo, H. G. Baldovi, M. T. Garcia Fernandez, S. Navalon, P. Atienzar, B. Ferrer, M. Alvaro, H. Garcia, Z. Li, *J. Phys. Chem. C* **2017**, *121*, 7015–7024.
[63] M. Lammert, C. Glißmann, N. Stock, *Dalt. Trans.* **2017**, *46*, 2425–2429.
[64] K. A. Lomachenko, J. Jacobsen, A. L. Bugaev, C. Atzori, F. Bonino, S. Bordiga, N. Stock, C. Lamberti, *J. Am. Chem. Soc.* **2018**, *140*, 17379–17383.
[65] D. Sun, W. Liu, M. Qiu, Y. Zhang, Z. Li, *Chem. Commun.* **2015**, *51*, 2056–2059.
[66] M. A. Nasalevich, C. H. Hendon, J. G. Santaclara, K. Svane, B. Van Der Linden, S. L. Veber, M. V. Fedin, A. J. Houtepen, M. A. Van Der Veen, F. Kapteijn, et al., *Sci. Rep.* **2016**, *6*, 1–9.
[67] H. Vrubel, T. Hasegawa, E. De Oliveira, F. S. Nunes, *Inorg. Chem. Commun.* **2006**, *9*, 208–211.
[68] S. Wongsakulphasatch, F. Nouar, J. Rodrigues, L. Scott, C. Le Guillouzer, T. Devic, P. Horcajada, J. . Greneche, P. Llewellyn, A. Vimont, et al., *Chem. Commun* **2015**, *51*, 10194–10197.
[69] M. Nyman, *Dalt. Trans.* **2011**, *40*, 8049–8058.
[70] H. T. Evans, *Inorg. Chem.* **1966**, *5*, 967–977.
[71] M. Aureliano, C. A. Ohlin, M. O. Vieira, M. P. M. Marques, W. H. Casey, L. A. E. Batista de Carvalho, *Dalt. Trans.* **2016**, *45*, 7391–7399.
[72] M. Matsumoto, Y. Ozawa, A. Yagasaki, Y. Zhe, *Inorg. Chem.* **2013**, *52*, 7825–7827.
[73] E. J. Graeber, B. Morosin, *Acta Crystallogr. Sect. B* **1977**, *33*, 2137–2143.
[74] R. Cao, T. M. Anderson, D. A. Hillesheim, P. Kögerler, K. I. Hardcastle, C. L. Hill, *Angew. Chemie Int. Ed.* **2008**, *47*, 9380–9382.
[75] R. Cao, T. M. Anderson, D. A. Hillesheim, P. Kögerler, K. I. Hardcastle, C. L. Hill, *Angew. Chemie Int. Ed.* **2008**, *47*, 9380–9382.
[76] U. Lee, H. C. Joo, K. M. Park, S. S. Mal, U. Kortz, B. Keita, L. Nadjo, *Angew. Chemie - Int. Ed.* **2008**, *47*, 793–796.
[77] H. C. Joo, K. M. Park, U. Lee, *Acta Crystallogr. Sect. E Crystallogr. Commun.* **2015**, *71*, 786–790.
[78] N. Vankova, T. Heine, U. Kortz, *Eur. J. Inorg. Chem.* **2009**, 5102–5108.
[79] J. H. Son, C. A. Ohlin, W. H. Casey, *Dalt. Trans.* **2013**, *42*, 7529–7533.
[80] W. Guo, J. Bacsa, J. Van Leusen, K. P. Sullivan, H. Lv, P. Kögerler, C. L. Hill, *Inorg. Chem.* **2015**, *54*, 10604–10609.
[81] N. Strukan, M. Cindrić, B. Kamenar, *Polyhedron* **1997**, *16*, 629–634.
[82] O. W. Howarth, L. Pettersson, I. Andersson, *J. Chem. Soc. Dalt. Trans.* **1989**, 1915–1923.
[83] M. Nyman, L. J. Criscenti, F. Bonhomme, M. A. Rodriguez, R. T. Cygan, *J. Solid State Chem.* **2003**, *176*, 111–119.
[84] J. Keggin, *Nature* **1933**, *131*, 908–909.
[85] D. M. P. Mingos, *Bonding and Charge Distribution in Polyoxometalates: A Bond Valence Approach.*, Springer, Berlin, **1999**.
[86] X. López, J. J. Carbó, C. Bo, J. M. Poblet, *Chem. Soc. Rev.* **2012**, *41*, 7537–7571.
[87] S. N. Britvin, I. V. Pekov, V. O. Yapaskurt, N. N. Koshlyakova, J. Göttlicher, S. V. Krivovichev, A. G. Turchkova, E. G. Sidorov, *Sci. Rep.* **2020**, *10*, 6345.
[88] K. Y. Monakhov, W. Bensch, P. Kögerler, *Chem. Soc. Rev.* **2015**, *44*, 8443–8483.
[89] A. Kondinski, T. Heine, K. Y. Monakhov, *Inorg. Chem.* **2016**, *55*, 3777–3788.
[90] L. K. Mahnke, A. Kondinski, U. Warzok, C. Näther, J. van Leusen, C. A. Schalley, K. Y. Monakhov, P. Kögerler, W. Bensch, *Angew. Chemie - Int. Ed.* **2018**, *57*, 2972–2975.
[91] C. Streb, in (Ed.: Y.-F. Song), Springer International Publishing, Cham, **2018**, pp. 31–47.
[92] L. C. W. Baker, V. S. Baker, K. Eriks, M. T. Pope, M. S. Orville, W. Rollins, J. H. Fang, L. L. Koh, *J. Am. Chem. Soc.* **1966**, *88*, 2329–2331.
[93] D. P. Smith, M. T. Pope, *Inorg. Chem.* **1973**, *12*, 331–336.
[94] M. T. Pope, T. F. Scully, *Inorg. Chem.* **1975**, 953–954.
[95] J. J. Altenau, M. T. Pope, R. A. Prados, H. So, *Inorg. Chem.* **1975**, *14*, 417–421.
[96] I. V Potapova, T. A. Karpukhina, L. P. Kazanskii, V. I. Spitsyn, *Bull. Acad. Sci. USSR, Div. Chem. Sci.* **1979**, *28*, 674–678.
[97] L. I. Kuznetsova, Y. V. Chernyshova, R. I. Maksimovskaya, *Inorganica Chim. Acta* **1990**, *167*, 223–231.
[98] I. Kawafune, G. Matsubayashi, *Chem. Lett.* **1992**, *21*, 1869–1872.
[99] M. A. Schwegler, J. A. Peters, H. van Bekkum, *J. Mol. Catal.* **1990**, *63*, 343–351.
[100] M. T. Pope, S. E. O'Donnel, R. A. Prados, in *Inorg. Compd. with Unusual Prop.*, **1976**, pp. 85–94.
[101] H. Chermette, F. Lefebvre, *Comptes Rendus Chim.* **2012**, *15*, 143–151.
[102] J. J. Cowan, A. J. Bailey, R. A. Heintz, B. T. Do, K. I. Hardcastle, C. L. Hill, I. A. Weinstock, *Inorg. Chem.* **2001**, *40*, 6666–6675.
[103] L. Pettersson, I. Andersson, J. H. Grate, A. Selling, *Inorg. Chem.* **1994**, *33*, 982–993.
[104] A. Selling, I. Andersson, J. H. Grate, L. Pettersson, *Eur. J. Inorg. Chem.* **2000**, *2000*, 1509–1521.
[105] I. Efremenko, R. Neumann, *J. Phys. Chem. A* **2011**, *115*, 4811–4826.
[106] W. Guan, L. Yan, Z. Su, S. Liu, M. Zhang, X. Wang, *Inorg. Chem.* **2005**, *44*, 100–107.
[107] C. Boskovic, *Acc. Chem. Res.* **2017**, *50*, 2205–2214.
[108] X. López, I. A. Weinstock, C. Bo, J. P. Sarasa, J. M. Poblet, *Inorg. Chem.* **2006**, *45*, 6467–6473.
[109] J. R. Winkler, H. B. Gray, in *Electron. Struct. Oxo-Metal Ions BT - Mol. Electron. Struct. Transit. Met. Complexes I* (Eds.: D.M.P. Mingos, P. Day, J.P. Dahl), Springer, Berlin, Heidelberg, **2012**, pp. 17–28.
[110] C. N. Kato, S. Negishi, K. Yoshida, K. Hayashi, K. Nomiya, *Appl. Catal. A Gen.* **2005**, *292*, 97–104.
[111] M. Sadakane, D. Tsukuma, M. H. Dickman, B. S. Bassil, U. Kortz, M. Capron, W. Ueda, *Dalt. Trans.* **2007**, 2833–2838.

[112] K. Nomiya, M. Takahashi, K. Ohsawa, J. A. Widegren, *J. Chem. Soc. Dalt. Trans.* **2001**, 2872–2878.
[113] F. Hussain, B. S. Bassil, L. H. Bi, M. Reicke, U. Kortz, *Angew. Chemie - Int. Ed.* **2004**, *43*, 3485–3488.
[114] G. S. Kim, H. Zeng, W. A. Neiwert, J. J. Cowan, D. VanDerveer, C. L. Hill, I. A. Weinstock, *Inorg. Chem.* **2003**, *42*, 5537–5544.
[115] X. Dong, S. Yang, B. Liu, P. Wu, H. Hu, G. Xue, *Inorg. Chem. Commun.* **2016**, *68*, 76–79.
[116] C. Ritchie, C. Streb, J. Thiel, S. G. Mitchell, H. N. Miras, D. L. Long, T. Boyd, R. D. Peacock, T. McGlone, L. Cronin, *Angew. Chemie - Int. Ed.* **2008**, *47*, 6881–6884.
[117] I. A. Weinstock, R. E. Schreiber, R. Neumann, *Chem. Rev.* **2018**, *118*, 2680–2717.
[118] K. Nakayama, M. Hamamoto, Y. Nishiyama, Y. Ishii, *Chem. Lett.* **1993**, *22*, 1699–1702.
[119] Y. V Geletii, A. . Shilov, *Kinet. Catal.* **1983**, *24*, 413–416.
[120] I. V. Kozhevnikov, *Chem. Rev.* **1998**, *98*, 171–198.
[121] L. El Aakel, F. Launay, A. Atlamsani, J. M. Brégeault, *Chem. Commun.* **2001**, *1*, 2218–2219.
[122] S. S. Wang, G. Y. Yang, *Chem. Rev.* **2015**, *115*, 4893–4962.
[123] W. Deng, Q. Zhang, Y. Wang, *Dalt. Trans.* **2012**, *41*, 9817–9831.
[124] R. Neumann, M. Levin, *J. Am. Chem. Soc.* **1992**, *114*, 7278–7286.
[125] M. T. Pope, S. E. O'Donnel, R. A. Prados, in *Inorg. Compd. with Unusual Prop.* (Ed.: R.B. King), American Chemical Society, **1976**, pp. 8–85.
[126] W. G. Klemperer, W. Shum, *J. Am. Chem. Soc.* **1978**, *100*, 4891–4893.
[127] W. Foun-, E. Station, P. J. Domaille, W. H. Knoth, *Society* **1983**, 818–822.
[128] X. López, C. Bo, J. M. Poblet, *J. Am. Chem. Soc.* **2002**, *124*, 12574–12582.
[129] E. Cadot, M. Fournier, A. Tézé, G. Hervé, *Inorg. Chem.* **1996**, *35*, 282–288.
[130] V. Prabhakaran, Z. Lang, A. Clotet, J. M. Poblet, G. E. Johnson, J. Laskin, *ACS Nano* **2019**, *13*, 458–466.
[131] H. D. Pratt, T. M. Anderson, *Dalt. Trans.* **2013**, *42*, 15650–15655.
[132] A. P. Ginsberg, *Inorganic Syntheses*, John Wiley & Sons, New York, **1990**.
[133] H.-Y. Chen, R. Al-Oweini, J. Friedl, C. Y. Lee, L. Li, U. Kortz, U. Stimming, M. Srinivasan, *Nanoscale* **2015**, *7*, 7934–7941.
[134] M. T. Pope, A. Muller, *Angew. Chemie Int. Ed. English* **1991**, *30*, 34–48.
[135] H. D. Pratt, W. R. Pratt, X. Fang, N. S. Hudak, T. M. Anderson, *Electrochim. Acta* **2014**, *138*, 210–214.
[136] J. J. Baldoví, A. Kondinski, *Inorganics* **2018**, *6*, 101.
[137] N. V. Izarova, A. Kondinski, N. Vankova, T. Heine, P. Jäger, F. Schinle, O. Hampe, U. Kortz, *Chem. - A Eur. J.* **2014**, *20*, 8556–8560.
[138] A. Kondinski, N. Vankova, F. Schinle, P. Jäger, O. Hampe, U. Kortz, T. Heine, *Eur. J. Inorg. Chem.* **2014**, 3771–3778.
[139] N. V. Izarova, Z. Lin, P. Yang, A. Kondinski, N. Vankova, T. Heine, U. Kortz, *Dalt. Trans.* **2016**, *45*, 2394–2398.
[140] Y. P. Jeannin, *Sect. Title Inorg. Chem. React.* **1998**, *98*, 51–76.

Table of Contents : Isomeric Polyoxometalates

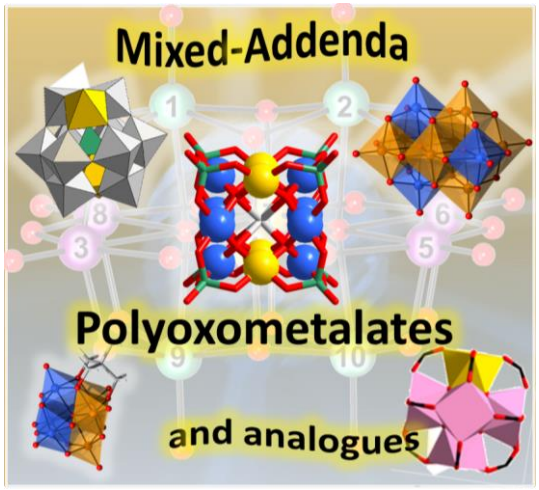

Polyoxometalates and their metal cluster analogues have been widely explored for use as catalysts in many different areas of chemistry, however through introduction of mixed metal components, their properties can be precisely tuned further. In this minireview we explore the relationship between mixed addenda isomers and their properties, experimentally and computationally, including the difficulties in controlling isomerism during synthesis.

Institute and/or researcher Twitter usernames: @POMtronics, @TPV_group, @KULeuvenChemie,